SHORT-TERM IRRADIANCE VARIABILITY
--
STATION PAIR CORRELATION AS A FUNCTION OF DISTANCE

Richard Perez
ASRC, 251 Fuller Rd
Albany, NY, 12203
Perez@asrc.albany,edu

Jim Schlemmer
ASRC, Albany, NY, 12203
Jim@asrc.cestm.albany,edu

Sergey Kivalov
ASRC, Albany, NY, 12203
skivalov@asrc.cestm.albany,edu

Karl Hemker, Jr.
ASRC, Albany, NY, 12203
kmh1@asrc.cestm.albany,edu

Thomas E. Hoff
Clean Power Research
Napa, CA 94558
tomhoff@cleanpower.com

ABSTRACT

In this article, we report on the correlation between the irradiance variability observed at two neighboring sites as a function of their distance, and of the considered variability time scale. Correlation is the factor that determines whether the combined relative fluctuations of two solar systems add up when correlation is high, or attenuate when correlation is low.

Using virtual networks in 24 US locations and cloud-motion derived from satellites as experimental evidence, we observe station pair correlations for distances ranging from 100 meters to 100 km and from variability time scales ranging from 20 seconds to 15 minutes.

Results show that the relationship between correlation, distance and time scale is predictable and largely independent of location and prevailing insolation conditions. Further, results indicate that the distance at which station pairs become uncorrelated is a quasi linear function of the considered time scale.

1. INTRODUCTION

The short-term variability of solar resource is perceived as a roadblock to the large scale deployment of solar power generation. This issue is the subject of several major research initiatives in the United Sates and internationally, e.g., [1, 2, 3, 4, 5].

In a recently published article, Hoff and Perez [6] advanced that the relative short-term variability of a fleet of identical PV generators decreases as the inverse of the square root of their number if the fluctuations of each system are uncorrelated. They defined relative short-term variability as the variability resulting from the fleet of systems, and quantified it by the standard deviation of the fleet's time series of changes in power output, normalized to the fleet's total capacity. More recently, Perez et al. [7] , building upon earlier work by Skartveit and Olseth [8], showed that short-term variability for a single system at a given point in time could be estimated from hourly satellite-derived irradiances data such as Solar Anywhere [9] or the NSRDB [10].

In this article we focus on station pairs, and investigate the correlation of their short-term variability as a function of their distance. A zero correlation would indicate that, per [6], their cumulative relative variability will be $1/\sqrt{2}$ times their individual relative variability. Further, the possible existence of negative correlation at some key distance would indicate that fluctuations tend to cancel out, as hypothesized in Hoff and Perez's optimum point.

2. METHODS

2.1 Experimental Data

Experimental measuring station pairs positioned at arbitrary distances and located in arbitrary climatic environments would constitute the ideal source of experimental data to undertake the present analysis. Unfortunately, this information is not fully available just yet. Although a few networks do exist where a partial validation of the present results will be possible, e.g., [11], the necessary dense solar resource grids are the drawing board or in the startup phase as of this writing -- e.g., [1, 2, 4].

However, as introduced by [6], there is an effective proxy to gridded networks of stations: virtual networks. A virtual network consists of a single high-frequency measuring station, from which virtual stations can be inferred if the cloud speed aloft, V, is known. Letting $I_t^{station}$ be the Irradiance measured at the station at time t, the irradiance at a neighboring virtual station, $I_t^{virtual}$ located at a distance L is given by:

$$I_t^{virtual} = I_{t_1}^{station} \quad (1)$$

with $t_1 = t - {}^{L}/_{V}$ (2)

The virtual network concept makes two limiting assumptions: (1) the virtual stations are located in the direction of the cloud motion vector; and (2) the cloud fields stay nearly unchanged as they transits over the stations, although signal compression or extension is possible due to evolving cloud speeds. The second assumption may be considered as conservative because cloud field deformation over time would intensify the uncorrelated character of a pair of stations' fluctuations. The first limitation's impact will have to be evaluated in a planned follow-on study by analyzing high resolution network data when these become available, and by analyzing high resolution satellite images.

High frequency GHI and DNI data were obtained for 24 measuring stations, including 17 stations in the ARM network [12] and 7 stations in the SURFRAD network [13]. The ARM stations record data at a rate of three measurements per minute (20-second data) while the SURFRAD stations record data at a rate of one measurement per minute (one-minute data). Fifteen months of data were analyzed for each station. A complete list of the stations is provided in Table 1.

Virtual networks were constructed around each station per equations (1) and (2) by using the time/site specific cloud speeds produced as part of SolarAnywhere's operational cloud motion irradiance forecasts [14]. Site-time specific cloud speeds are derived by minimizing the RMSE of consecutive satellite images. This approach was first described and implemented by [15]. The cloud speeds have an operational frequency of one per hour. For the present analysis the cloud speed associated with each high frequency ground measurement was obtained via linear interpolation of the hourly speeds. Figure 1 illustrates the hourly cloud speeds derived for a sample high variability

TABLE 1: Experimental data

	Station	Latitude	Longitude	Elevation	Climate	Time Span
ARM NETWORK	ARM-E27	35.27	96.74	386 m	continental	1/09 - 4/10
	ARM-E19	35.56	98.02	421 m	continental	1/09 - 4/10
	ARM-E20	35.56	96.99	309 m	continental	1/09 - 4/10
	ARM-E21	35.62	96.07	240 m	continental	1/09 - 4/10
	ARM-E15	36.43	98.28	418 m	continental	1/09 - 4/10
	ARM-C1	36.61	97.49	318 m	continental	1/09 - 4/10
	ARM-E13	36.61	97.49	318 m	continental	1/09 - 4/10
	ARM-E12	36.84	96.43	331 m	continental	1/09 - 4/10
	ARM-E16	36.06	99.13	602 m	continental	1/09 - 4/10
	ARM-E11	36.88	98.29	360 m	continental	1/09 - 4/10
	ARM-E10	37.07	95.79	248 m	continental	1/09 - 4/10
	ARM-E9	37.13	97.27	386 m	continental	1/09 - 4/10
	ARM-E7	37.38	96.18	283 m	continental	1/09 - 4/10
	ARM-E6	37.84	97.02	409 m	continental	1/09 - 4/10
	ARM-E4	37.95	98.33	513 m	continental	1/09 - 4/10
	ARM-E1	38.20	99.32	632 m	continental	1/09 - 4/10
	ARM-E2	38.31	97.30	450 m	continental	1/09 - 4/10
SURFRAD NETWORK	Goodwin Creek	34.25	89.87	98 m	subtropical	1/09 - 4/10
	Desert Rock	36.63	116.02	1007 m	Arid	1/09 - 4/10
	Bondville	40.05	88.37	213 m	Continental	1/09 - 4/10
	Boulder	40.13	105.24	1689 m	Semi-arid	1/09 - 4/10
	Penn State	40.72	77.93	376 m	humid continental	1/09 - 4/10
	Sioux Falls	43.73	96.62	473 m	Continental	1/09 - 4/10
	Fort Peck	48.31	105.10	634 m	Continental	1/09 - 4/10

day at the ARM central facility, superimposed upon the station's measured GHI.

2.2 Quantifying station pair variability correlation

Hoff and Perez [6] quantified the relative short-term variability of a fleet of N solar generators as:

$$\sigma_{\Delta t}^{\Sigma N} = \left(\frac{1}{C^{Fleet}}\right)\sqrt{Var\left[\sum_{n=1}^{N}\Delta \boldsymbol{P}_{\Delta t}^{\boldsymbol{n}}\right]} \qquad (3)$$

Where C^{Fleet} is the total installed peak power of the fleet and $\Delta \boldsymbol{P}_{\Delta t}^{\boldsymbol{n}}$ is a random variable that represents the time series of changes in power at the nth PV installation using a sampling time interval of Δt.

In this article, we focus our attention on the changes in the clearness index ΔKt*instead of the changes in power output ΔP. Kt* is the ratio between GHI and clear sky global irradiance, GHI_{clear}. As such, Kt* embodies the relative characteristics of flat plate PV systems' output fluctuations. For the present analysis, it offers two advantages: (1) normalizing variability to unity, and (2) removing the effect of solar geometry which is a source of variability, albeit fully predictable, as Δt increases. The ΔKt* random variable time series is illustrated at the bottom of Figure 1 for Δt = 20 seconds and 15 minutes.

The station pair correlation between the two random variables $\Delta Kt_{\Delta t}^{*\,station}$ and $\Delta Kt_{\Delta t}^{*virtual}$ is calculated independently for each day and each virtual network for virtual station distances ranging from 100 m to 100 km, and for sampling intervals of 20 seconds (only for the ARM-based networks), 1 minute, 5 minutes and 15 minutes. Longer time intervals are not investigated since variability questions pertaining to longer time scales can already be addressed today by analyzing existing gridded satellite-derived data sets

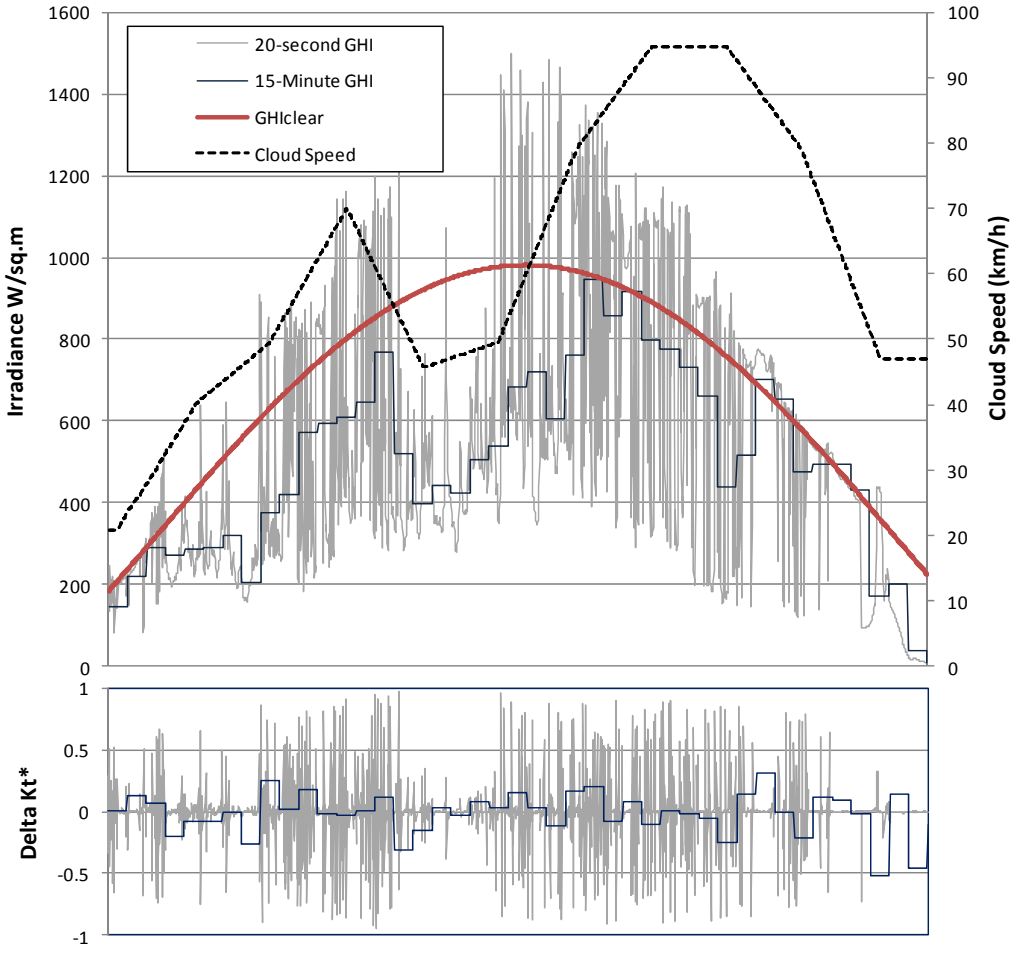

Figure 1: Sample high-variability day in the ARM network, showing 20-second GHI, 15 minute GHI and hourly interpolated cloud speeds.

For a given pair of stations extracted from one of the 24 virtual networks, for a given day j, a given time interval Δt, and a given distance L, the station pair correlation, $Cor_{\Delta tj}^{L}$ is calculated from all high frequency data points in that day for solar elevations in excess of 10°.

For that network location, the prevailing station pair correlation, $Cor_{\Delta tj}^{L}$, is derived as the weighted mean of each individual day's correlations. The weighting factor is the day's variability quantified by the daily variance of $\Delta Kt_{\Delta t,j}^{*}$.

$$Cor_{\Delta t}^{L} = \frac{\sum_{j=1}^{n}(Cor_{\Delta tj}^{L} * Var\left[\Delta Kt_{\Delta t,j}^{*}\right])}{\sum_{j=1}^{n} Var\left[\Delta Kt_{\Delta t,j}^{*}\right]} \quad (4)$$

where n is the total number of station-days analyzed.

3. RESULTS

The objective is to understand how station pair correlation varies as a function of distance and the considered sampling interval.

Starting with the observation of the relationship obtained from one day's worth of observations at one of the virtual network, we proceed with analyzing the composite trend resulting from all the days analyzed at that same network location per equation (4), investigating how the single day's relationship evolves. Finally we observe how the relationship further evolves when all 24 virtual network locations are considered.

3.1 Single virtual network, single day example

For the single day example we selected a highly variable day for the ARM central facility, April 19, 2009, illustrated in Figure 1.

The virtual station pair covariance for that day is plotted in Figure 2 as a function of distance for each sampling interval.

Correlation reaches zero at respectively 350 m, 800 m, 2.7 km and 7.8 km for sampling intervals of 20 s, 1 min, 5 min and 15 min. Beyond the zero crossover, the considered station pairs do not exhibit any significant positive correlation. It is interesting to note that in each case, correlation becomes slightly negative beyond the zero crossover point. The negative correlation indicates that at some distance on that day (respectively 600 m, 1km, 5km and 10 km for Δt of 20 s, 1 min, 5 min and 15 min) the effect of the passing clouds resulted in a partial cancelation of fluctuations, when the succession of cloudy and sunny periods tended to be in opposition of phase for all time scales at the two sites. This negative correlation effect might be traceable to the one dimensional nature of the virtual network and will have to be investigated further when 2-dimensional real network data become available.

3.2 Single virtual network, all data

Figure 3 is similar to figure 2, but the results are based on all 452 days analyzed at the ARM central facility. The solid line is obtained by application of equation (4) to individual days' correlations, i.e., applying weight as a function of each day's variability as quantified by the variance of the GHI index. Figure 3 also reports the standard deviation around the mean trend.

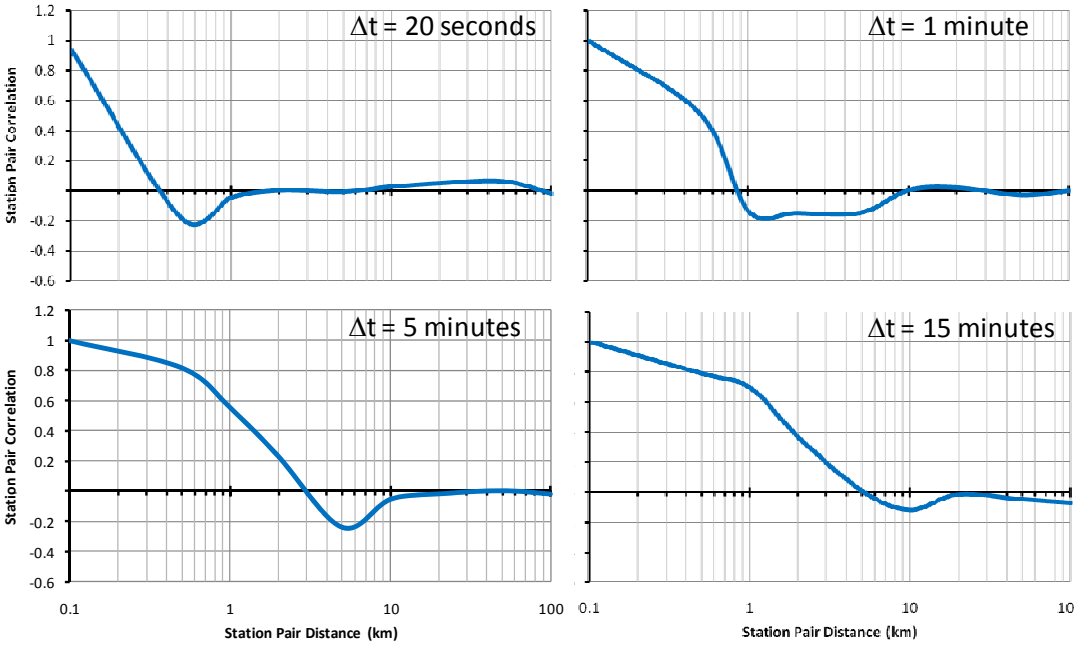

Figure 2: Single virtual network, single day station pair correlation as a function of distance and time scale

The resulting trace is robust, crossing the zero correlation threshold at respectively 400m, 850 m, 3 km and 9 km for each considered sampling intervals, i.e., remarkably close to the single day example shown above. The tightness of the standard deviation indicates that individual events do not depart significantly from the trend, particularly for shorter sampling intervals (20s and 1 min).

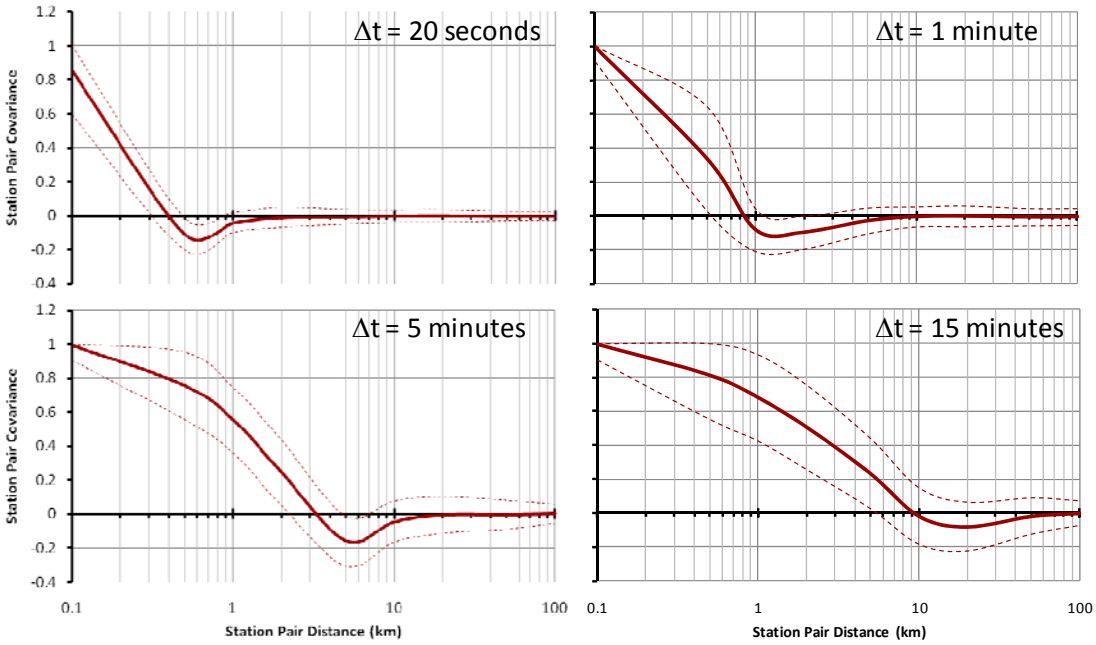

Figure 3: Single virtual network's mean station pair correlation trends resulting from 15 months of data

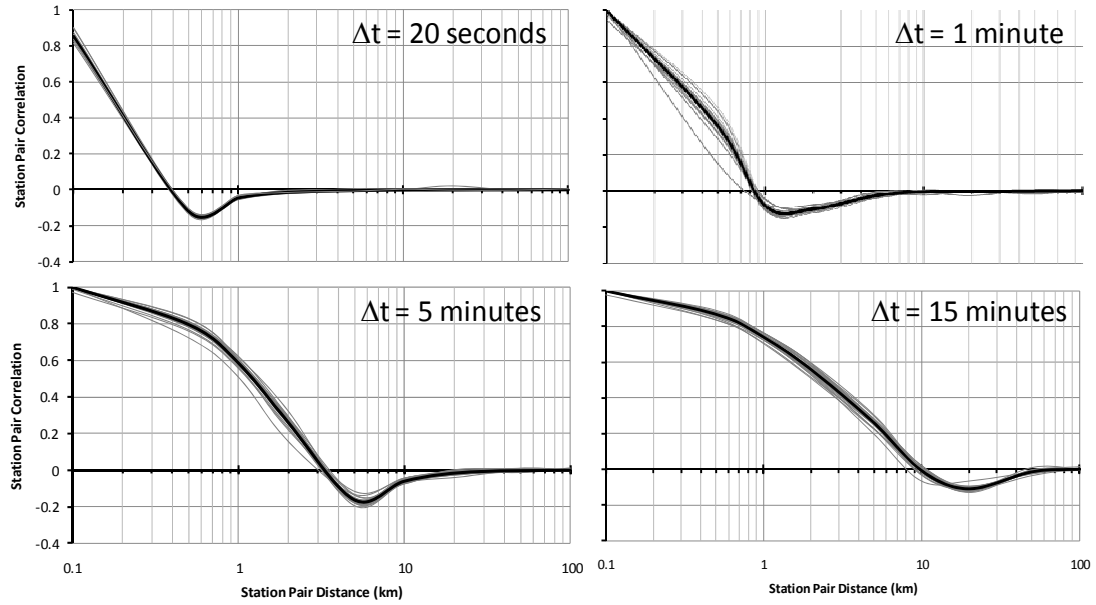

Figure 4: Station pair correlation trends resulting from all virtual networks and 15 months of data. Thin gray lines represent individual networks.

Interestingly, the resulting trend for the ARM site conserves the small negative correlation peak observed for the individual day, despite the differing cloud speeds and cloud shapes that occurred each hour of each day.

3.3 All virtual networks, all data

Figure 4 is similar to figures 2 and 3, but includes all data points analyzed at all locations (i.e., nearly 17 million 20 second data points). The resulting heavy line is the 24-network mean (only 17 networks for $\Delta T = 20$ s). Individual networks are represented by the thin gray lines.

The agreement between all networks, including nearly identical zero cross-over points and negative correlation peaks, is remarkable given the diversity of possible weather conditions and cloud variability drivers in highly differing climatic environments.

4. DISCUSSION

The virtual network analysis undertaken here on a large array of climatic environments, weather drivers, and seasonal conditions leads to a remarkably well defined set of trends linking distance, fluctuation frequency and station pair correlation.

The evidence from this exhaustive analysis suggests that 20 second fluctuations become uncorrelated positively at a distance of less than 500 meters. The distances are respectively 1 km, 4 km and 10 km for fluctuation time scales of 1, 5 and 15 minutes respectively.

The relationship between the zero correlation cross-over distance and Δt is quasi linear as can be seen in Figure 5. This quasi-linearity substantiates the concept of the dispersion factor introduced earlier by [6] which embodies time scale, cloud speed and distance into one single parameter determining variability. Ongoing studies by Mills & Wiser [16] and Hoff & Perez [17] would indicate that the linear relationship could be extended at either end of the current Δt span to estimate station pair correlation for other time scales.

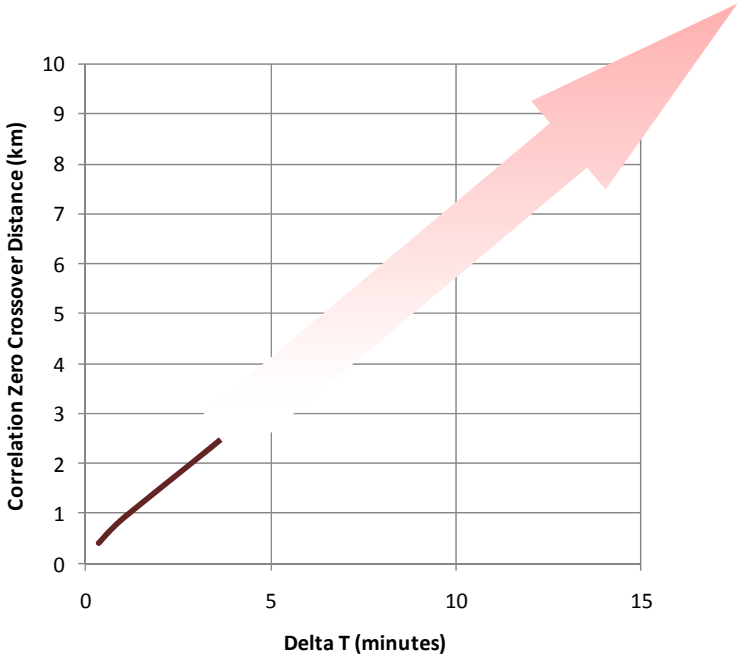

Figure 5: zero correlation crossover distance as a function of fluctuation time scale

Extrapolating the present results to the case of a homogeneously dispersed solar resource in a metropolitan area such as the greater New York City area (40x40 km) suggests that the high frequency (20 second) variability experienced by a single small system should be reduced by a factor of 80 when considering the entire metropolitan area . The variability reduction would become smaller as the considered frequency increases: the metropolitan variability would be reduced by respectively 40, 10 and 4 for fluctuation time scales of 1, 5 and 15 minutes. This example is illustrated in Figure 6, comparing the $\Delta K t^*_{\Delta t}$ time series of a single installation to that of a homogeneous hypothetical deployment of systems over a 40x40 km area.

The findings of this study are consistent with limited evidence assembled from measurement station pairs – e.g., see [16], Soubdhan & Calif, [18], Murata et al., [20] -- However these station pairs are too far apart to provide an exhaustive validation, hence the present findings will have to be substantiated by follow-on work. In particular, Clean Power Research recently deployed a low-cost 25-station modulable network in Central California designed to capture the relative ΔGHI data streams down to scales of 10 second (Hoff & Perez, 2010b). Further, as a planned next step of this work, we will analyze high resolution (1 km) satellite images and apply the cloud motion forecast algorithm (Perez et al., 2010b) to simulate high resolution, high frequency irradiance time series over any arbitrary extended area.

We will use these upcoming bottom-up and top-down experimental data to verify, and as needed adjust, the present virtual network-derived results. It is possible that these future two dimensional network verifications will produce slightly different results -- in particular the negative correlation peak observed for all sites and time scales is likely to be reduced or disappear, as it might be an artifact of the one-dimensionality of the present virtual networks. However the absence of correlation occurring consistently at all sites beyond a given distance for a given time scale should hold.

5. ACKNOWLEDGEMENT

This study was funded by Clean Power research under a California Solar Initiative (CSI) Grant Agreement titled “Advanced Modeling and Verification for High Penetration PV.” The California Public Utilities Commission is the Funding Approver, Itron is the Program Manager, and the California IOUs are the Funding Distributors

6. REFERENCE

1. BNL, Brookhaven National Laboratory, (2010): Personal Communication -- Overview of BNL’s Research Agenda on Solar Energy. BNL, Upton, NY
2. CSI, California Solar Initiative R&D Program, (2010): California Public Utility Commission, San Francisco, CA
3. USDOE, US Department of Energy, (2009): Recovery Act: High Penetration Solar Deployment R&D program. http://www1.eere.energy.gov/solar/financial_opps_detail.html?sol_id=286

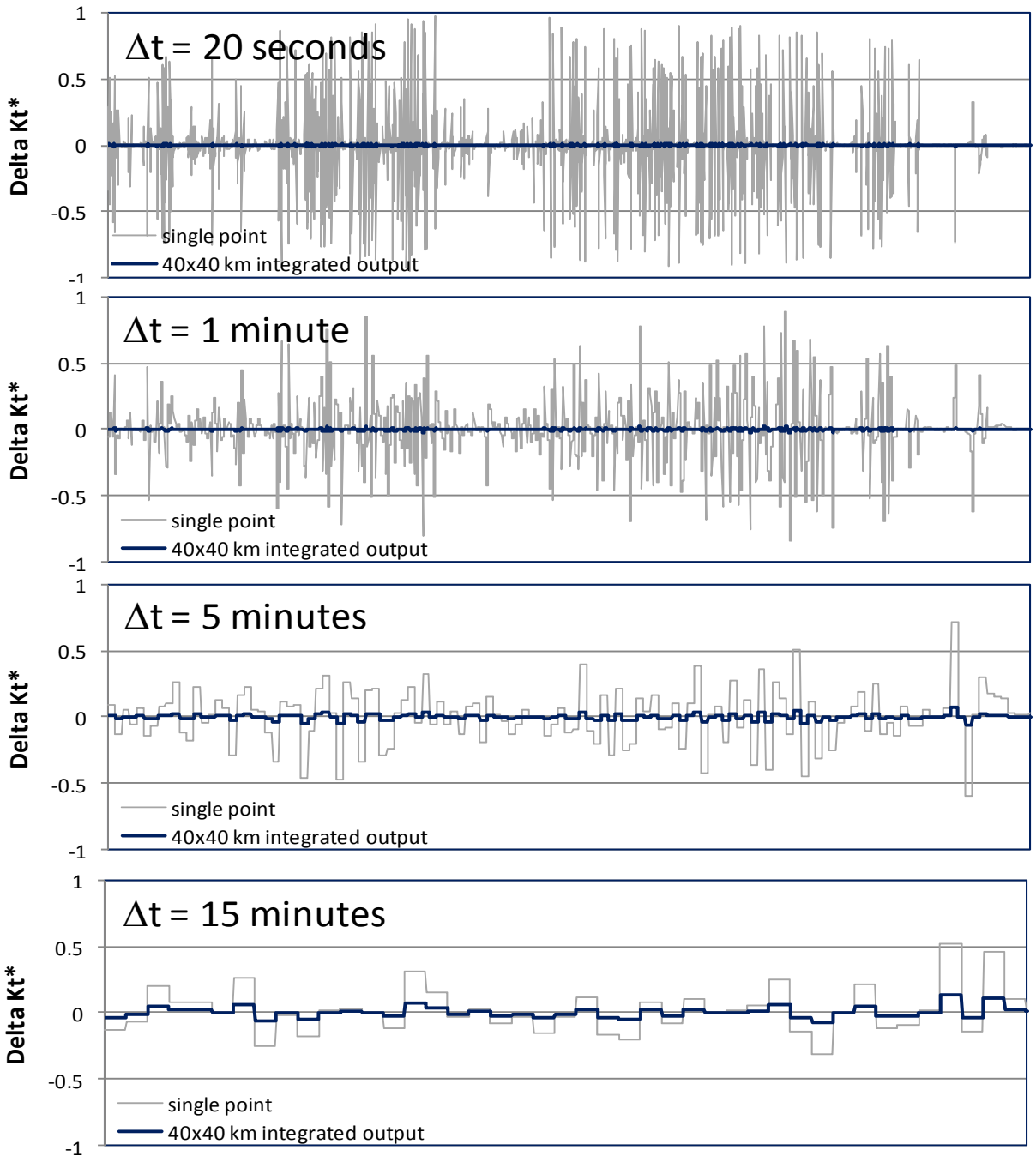

Figure 6: Comparing single site and 40kmx40km extended variability for different fluctuation time scales

4. Rawson, (2010): solar and the smart grid session SPI 2010.
5. IEA Solar Heating and Cooling Programme, (2010): Task 46 – Solar Resource Assessment and Forecasting, Subtask A - Resource Applications for High Penetration of Solar Technologies. International Energy Agency, Paris, France.

6. Hoff T., and R. Perez, (2010): Quantifying PV Power Output Variability. Solar Energy 84, 10, 1782-1793
7. Perez R., S. Kivalov, J. Schlemmer, K. Hemker Jr., and T. Hoff (2010a): Parameterization of Site-Specific Short-Term Irradiance Variability, Submitted to Solar Energy
8. Skartveit A., and J. A. Olseth, (1992): The Probability Density of Autocorrelation of Short-term Global and beam irradiance. Solar Energy, Volume 46, No. 9, pp. 477-488.
9. Solar Anywhere, (2010): www.solaranywhere.com
10. NSRDB, (1998-2005): http://rredc.nrel.gov/solar/old_data/nsrdb/1991-2005/
11. Kleissl, J., 2009: http://maeresearch.ucsd.edu/kleissl/demroes/map.html
12. Stokes, G. M., and S. E. Schwartz (1994): The Atmospheric Radiation Measurement (ARM) Program: Programmatic Background and Design of the Cloud and Radiation Test bed, Bulletin of American Meteorological Society, 75, 1201-1221
13. SURFRAD Network (2010): Monitoring Surface Radiation in the Continental United States, www.srrb.noaa.gov/surfrad/
14. Perez R., S. Kivalov, J. Schlemmer, K. Hemker Jr., D. Renne and T. Hoff (2010b) : Validation of Short and Medium Term Operational Solar Radiation Forecasts in the US. Solar Energy 84, 12, 2161-2172
15. Lorenz, E., Hammer, A., Heinemann, D.: 2004, 'Short term forecasting of solar radiation based on satellite data', EUROSUN2004 (ISES Europe Solar Congress), Freiburg, Germany
16. Mills A. and R. Wiser, (2010): Implications of Wide-Area Geographic Diversity for Short-Term Variability of Solar Power. LBNL Report No. 3884E
17. Hoff, T., and R. Perez (2010): PV Power Output Variability: Calculation of Correlation Coefficients Using Satellite Insolation Data. Proc. Solar 2011, ASES Annual Conference, Raleigh, NC
18. Soubdhan T., and R. Calif, (2010) : Spatio-Temporal Analysis of Solar Radiation Measured at Two Sites in Guadeloupe. EuroSun 2010 Conference, Graz, Austria
19. Murata, A., H. Yamaguchi, and K. Otani (2009): A Method of Estimating the Output Fluctuation of Many Photovoltaic Power Generation Systems Dispersed in a Wide Area, Electrical Engineering in Japan, Volume 166, No. 4, pp. 9-19